Molecular dynamics study of slip at the interface between immiscible polymers

Sandra Barsky and Mark O. Robbins
Department of Physics and Astronomy, Johns Hopkins University, Baltimore, Maryland 21218
(Received 18 October 2000; published 24 January 2001)

Nonequilibrium molecular dynamics simulations were used to study the structural properties and viscous response of interfaces in binary blends of symmetric polymers. The polymers were made immiscible by increasing the repulsion between unlike species. As the repulsion increased, the interface narrowed, and the fraction of chain ends in the interfacial region increased. The viscosity in the interfacial region η_I was lower than the bulk viscosity, leading to an effective slip boundary condition at the interface. As the degree of immiscibility increased, the interfacial viscosity decreased, and the slip length increased. When the radius of gyration of the chains was much larger than the interfacial width, η_I was independent of chain length. As predicted by de Gennes and co-workers, η_I corresponds to the bulk viscosity of chains whose radius of gyration is proportional to the width of the interfacial region.

DOI: 10.1103/PhysRevE.63.021801 PACS number(s): 83.80.Tc, 83.50.Lh, 83.10.Rs

I. INTRODUCTION

Polymer blends have tremendous technological applications, since blending allows one to create new materials with tunable properties. However, dissimilar polymers generally become immiscible as the number of monomers N increases. The resulting phase separation creates many interfaces between regions of different composition. The static and dynamic properties of these interfaces have strong effects on the material properties and processing of the blend.

A large body of theoretical work has been dedicated to understanding the properties of polymer interfaces [1–7]. Most of the analytic work is based on the Flory-Huggins model. The degree of immiscibility is characterized by the well-known interaction parameter χ [1], which corresponds to the enthalpic cost for placing a monomer of one species in a homogeneous phase of the other species. Chains become immiscible when N is large compared to $1/\chi$. Many predictions of this model have been tested by recent simulations, including the structural properties of equilibrium interfaces [8] and critical behavior [9].

In this paper we examine the nonequilibrium response of polymer interfaces to a tangential flow field. This allows us to test predictions about the interfacial viscosity and the degree of slip at polymer/polymer interfaces [4,5,7]. We focus on the most studied case of a symmetric, binary blend where the two polymers A and B have the same length, density, and viscosity, but are immiscible. The chains are short enough to be in the Rouse limit [10], and the linear response at low shear rates is calculated.

The equilibrium properties of such polymer interfaces are well studied. For a static interface located at $z=0$, Helfand and Tagami found that the volume fraction of species A has the form [3]

$$\phi_A(z)=1-\phi_B(z)=\frac{e^{2z/a_I}}{e^{2z/a_I}+e^{-2z/a_I}}, \tag{1}$$

where a_I is the interfacial width. By comparing the enthalpic cost and entropy gain when a loop of length s of A enters the B rich region, one finds that the typical length of loops scales as $s^*=1/\chi$. The interfacial width scales as twice the radius of gyration R_g of a chain of length s^*, giving $a_I=2b/\sqrt{6\chi}$ [7]. Here b is the statistical segment length, and is related to R_g and the root mean squared end-to-end distance R_{ee} by $b=R_g\sqrt{6/N}=R_{ee}/\sqrt{N}$ in the large N limit.

The bulk viscous response of polymers is also well established. Chains that are shorter than the entanglement length N_e exhibit Rouse dynamics. The bulk viscosity rises linearly with chain length: $\eta_B=\zeta b^2 N/\nu_0$, where ζ is the monomer friction coefficient and ν_0 is the monomer volume [10]. de Gennes and co-workers have argued that the viscosity in the interfacial region η_I should be given by the Rouse formula, but with the typical loop length s^* replacing N. The idea is that only segments of this length need to move in order to relax stress in the interfacial region. If s^* is much less than N, or equivalently a_I is much less than R_g, then $\eta_I=\zeta b^2 s^*/\nu_0=\zeta b^2/\nu_0\chi=\zeta 3a_I^2/2\nu_0$. Since this expression is independent of N, while η_B rises linearly with N, there will be an increasing amount of slip at the polymer interface as N increases [5,7]. Slip becomes even more pronounced if N becomes longer than the entanglement length [4,5,7], but this limit is not considered here.

Goveas and Fredrickson have recently used the Fokker-Planck equation to provide a more formal derivation of the relation between interfacial width and interfacial viscosity [7]. They construct a constitutive equation for stress relaxation near the interface between Rouse chains, and solve for the shear stress in response to a weak shear. The resulting viscosity varies with the distance from the interface as

$$\frac{\eta(z)}{\eta_B}=\left[1+\frac{R_{ee}^2}{a_I^2}16\phi_A(z)\phi_B(z)\right]^{-1}, \tag{2}$$

where $\phi_{A,B}(z)$ are the equilibrium concentration profiles [Eq. (1)]. In the limit of small a_I the viscosity at $z=0$ can be expanded to give

$$\eta_I\equiv\eta(0)=\frac{1}{4}\zeta a_I^2/\nu_0=\frac{1}{6}\zeta b^2 s^*/\nu_0. \tag{3}$$

Thus Goveas and Fredrickson obtain the same scaling as de Gennes and co-workers in this limit. However their prefactor is quite small since Eq. (3) gives the viscosity of a Rouse chain with length $s^*/6$.

To test the above predictions for the interfacial viscosity, one must work at low enough shear rates to avoid shear thinning. The interface must also be sharp, $s^* \ll N$, so that the effective chain length in the interface is not limited by N. In addition, N and s^* must be long enough to exhibit Gaussian behavior, but less than N_e so that the chains are in the Rouse limit. This leaves a relatively narrow range of N where scaling can be studied.

In order to maximize the scaling regime, we consider a standard model of polymer melts [11] that gives a large ratio between the entanglement and persistence length. Species A and B are identical, but an extra repulsive term between them makes them immiscible [12,13]. To impose shear, solid bounding walls that are parallel to the A-B interface are displaced tangentially at constant relative velocity. The interface width, chain statistics, and viscosity are measured as a function of distance from the interface.

When the added repulsion is small, the interface width is larger than the radius of gyration R_g of bulk polymers. In this limit, $\eta_I \approx \eta_B$ and there is little slip at the interface. As the degree of repulsion increases, the interface becomes much sharper, and the viscosity of the interface becomes independent of N. The viscosity is qualitatively consistent with Goveas and Fredrickson's expressions [Eqs. (2) and (3)] [7], but the prefactor for η_I is closer to the value obtained by de Gennes and co-workers [5].

The paper is organized as follows. In the next section we review the interaction potentials and simulation techniques used in this work. Results and analyses are presented in Sec. III, and Sec. IV provides a summary and conclusions.

II. MODEL

We use Kremer and Grest's bead-spring model for linear-chain molecules [11]. Spherical monomers of mass m are linked into chains of length N by a nearest-neighbor interaction potential

$$U_{nn}(r_{ij}) = \begin{cases} -\frac{1}{2} k R_0^2 \ln[1-(r_{ij}/R_0)^2], & r_{ij} < R_0 \\ \infty, & r_{ij} \geqslant R_0, \end{cases} \tag{4}$$

where r_{ij} is the distance between monomers i and j, $R_0 = 1.5\sigma$, $k = 30\epsilon/\sigma^2$, and σ and ϵ set the length and energy scales, respectively. The characteristic time scale is $\tau = \sigma\sqrt{m/\epsilon}$. Typical values of ϵ, σ, and τ for hydrocarbon chains would be of order 30 meV, 0.5 nm, and 3 ps, respectively [11,14]. All monomers interact through a truncated Lennard-Jones (LJ) potential

$$U_{LJ}(r_{ij}) = \begin{cases} 4\epsilon_{\alpha\beta}[(\sigma/r_{ij})^{12} - (\sigma/r_{ij})^6], & r_{ij} < r_c \\ 0, & r_{ij} \geqslant r_c. \end{cases} \tag{5}$$

where the interaction energy $\epsilon_{\alpha\beta}$ depends on the types α and β of monomers i and j.

To make a symmetric blend of immiscible polymers we follow the work of Grest, Lacasse and co-workers [12,13]. The LJ potential is truncated at $r_c = 2^{1/6}$ so that monomer interactions are strictly repulsive. Two monomers of the same type interact with $\epsilon_{AA} = \epsilon_{BB} = \epsilon$. An extra repulsion is added between unlike monomers $\epsilon_{AB} = \epsilon_{BA} = \epsilon(1+\epsilon^*)$. Increasing ϵ^* increases χ, although the relation is nonlinear. Results are presented for ϵ^* between 0.37 and 3.2, and chains of length $N = 8$, 16, 32, and 64. All but the shortest chains were immiscible over the entire range of ϵ^*. The longest chain length is slightly below the best estimate for the entanglement length $N_e = 74 \pm 9$ of the bead-spring model [15,16].

The polymer is confined in a simulation cell that is periodic in the x and y directions, and bounded by two walls in the z direction. Each wall contains $N_W = 1600$ atoms that are tethered to the sites of a (1,1,1) surface of a fcc lattice by harmonic springs of stiffness $\kappa = 1320\epsilon\sigma^{-2}$. The wall atoms do not interact with each other, and have identical interactions with the two types of monomer. These are described with a LJ potential with an attractive tail $r_c = 1.5\sigma$, an increased energy scale $\epsilon_{WA} = \epsilon_{WB} = 1.7\epsilon$, and the same length scale σ. These parameters were chosen to limit the amount of slip at the walls [17–19].

For the results presented below, the walls are separated by $L_z = 49.0\sigma$, and the periods along x and y are $L_x = 38.5\sigma$ and $L_y = 33.4\sigma$, respectively. There are 49 152 monomers giving a mean density of $\rho \equiv 1/v_0 \approx 0.80\sigma^{-3}$ in the center of the cell. There are well-studied density modulations near each wall that are not of interest here [17–20]. We exclude the first 5σ near each wall from our analysis routines in order to avoid their influence. The remaining thickness of each type of polymer is much larger than the end-to-end distances in Table I. From the quoted values of R_g and R_{ee} we obtain a value of the statistical segment length $b = 1.28\sigma$ that is consistent with previous work [11,15].

The initial condition is created from an equilibrated system of identical chains at the simulation temperature $k_B T/\epsilon = 1.1$. Polymers whose centers of mass are in the bottom half of the simulation box are labeled A, and the remaining half of the polymers are labeled B. The equations of motion are then integrated using a fifth-order predictor-corrector method [14], with a time step $\delta t = 0.0075\tau$. The system is allowed to equilibrate for 1125τ. After this time interval the interface width and other parameters have reached a steady state.

Shear flow in the polymer melt is induced by moving the top wall at a constant speed v_W in the x direction. Constant temperature is maintained by adding a Gaussian white noise and damping to the equations of motion [11,17]. These terms are only added in the y and z directions to avoid affecting the flow profile. Once the system has reached steady state, the local shear rate $\dot{\gamma}(z) \equiv \partial v_x/\partial z$ is calculated as a function of z. This is done by dividing the system into slices of width 0.095σ parallel to the x-y plane and calculating the average velocity of the monomers within these slices over $(9000-15\,000)\tau$. A finite difference is then taken to give the local $\dot{\gamma}$, and the results are smoothed by taking a running

TABLE I. Sizes of the interface and polymer. The range of z over which the concentration of A monomers changes from 75% to 25% or 90% to 10% is denoted by $w(75)$ or $w(90)$, respectively. The ratio of these values is consistent with Eq. (1) and they were used to calculate a_I. Uncertainties in these widths are less than 5% except where otherwise indicated. The values of the radius of gyration R_g and the end-to-end distance R_{ee} for polymers of length $N=8$ to 64 are included for comparison.

		Interface width			Chain size	
N	ϵ^*	$w(75)/\sigma$	$w(90)/\sigma$	a_I/σ	R_g/σ	R_{ee}/σ
64					4.71	11.87
	0.37	2.3	4.5	4.1		
	0.6	1.8	3.6	3.3		
	1.2	1.7	3.2	3.0		
	3.2	1.4	2.7	2.5		
32					2.96	7.20
	0.37	2.8	5.3	5.0		
	0.6	2.1	4.1	3.8		
	0.8	2.2	4.2	3.9		
	1.2	1.9	3.7	3.4		
	2.2	1.6	3.0	2.7		
	3.2	1.4	2.6	2.4		
16					2.01	4.98
	0.37	3.0 ± 0.2	6.5 ± 0.2	5.8 ± 0.2		
	0.6	2.8	5.5	5.1		
	0.8	2.2	4.6	4.1		
	1.2	1.9	3.6	3.3		
	3.2	1.6	3.1	2.9		
8					1.30	3.14
	0.8	4.0	9 ± 2	7.4 ± 0.4		
	1.2	2.5	5.4	4.7		
	3.2	1.6	3.0	2.8		

average over ten slices. The local viscosity of the fluid is then obtained from the relation

$$\eta(z)=\frac{P_{xz}}{\dot{\gamma}(z)} \tag{6}$$

where the shear stress P_{xz} is independent of z once the system is in steady state [21].

In this paper we are interested in the Newtonian regime of flow, before the onset of shear thinning. Since the onset of shear thinning moves to lower shear rates as chain length increases [22], lower wall velocities must be used for larger N. However, increasing N also lowers the shear rate at fixed wall velocity, because the amount of slip at the walls increases [19]. For the results presented below we use $v_W=0.5\sigma/\tau$ with $N=8$ and 16, and $v_W=0.1\sigma/\tau$ with $N=32$ and 64. This produces the following shear rates in the bulk fluid regions (away from all interfaces):

$$\dot{\gamma}_B=\frac{\partial v_x}{\partial z}=\begin{cases} 0.0092\pm0.0002, & N=8 \\ 0.0082\pm0.0002, & N=16 \\ 0.0013\pm0.0001, & N=32 \\ 0.000\,93\pm0.000\,07, & N=64, \end{cases} \tag{7}$$

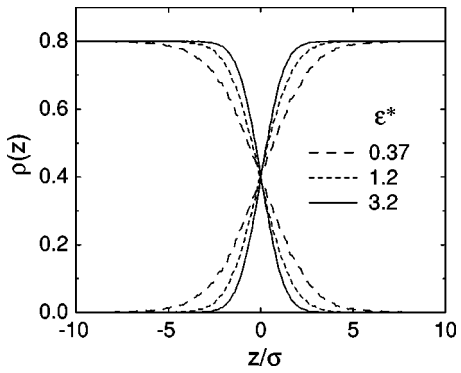

FIG. 1. Monomeric density of $N=32$ chains as a function of height z for the indicated values of ϵ^*. The curves for monomers of type A (B) approach 0.8 at small (large) z. The interface becomes significantly sharper as ϵ^* increases. Only the region near the interface is shown.

where the quoted statistical error bars are comparable to variations with ϵ^*.

III. RESULTS

A. Interface width and chain end statistics

A key parameter in analytic theories of interfacial viscosity is the width of the interface between immiscible polymers [5,7]. To determine this quantity we calculated the density $\rho_{A,B}(z)$ of each species of monomer in slices of width 0.095σ parallel to the x-y plane. The resulting density profiles for chains of length $N=32$ are plotted in Fig. 1 for three values of the immiscibility parameter ϵ^*. The interface clearly becomes narrower as ϵ^* increases.

To quantify this trend we determined $w(75)$ and $w(90)$, the ranges of z over which the concentration of A changed from 75% to 25% or 90% to 10%, respectively. These values are listed in Table I. If the analytic expression for the density profile in Eq. (1) is correct, then $w(75)=0.549a_I$, and $w(90)=1.099a_I$ should be almost exactly twice as large. Our measured values of w are consistent with this factor of 2, and were used to determine the values of a_I in Table I. Note that capillary waves can increase the intrinsic width given by Flory-Huggins theory [13,23]. This has been considered in detail by Lacasse, Grest and Levine [13] for the model used here. The effect decreases with surface tension and thus with ϵ^*. It is a small effect for the parameters considered here, and is smallest in the regime where the interfacial viscosity saturates (see below).

Theoretical conclusions about the interfacial viscosity [5,7] depend on the interface width becoming independent of chain length once the radius of gyration becomes large compared to a_I. The results in Table I show that a_I becomes relatively independent of N even when R_g/a_I is only of order 1/2. For example, at $\epsilon^*=3.2$ the interface width changes only from 2.8σ to 2.4σ while R_g changes from 1.3σ to 4.7σ. We will see that the interfacial viscosity is more sensitive to the value of N than is a_I.

It has been argued by Helfand, Bhattacharjee, and Fredrickson [24] that polymer ends lie preferentially at the in-

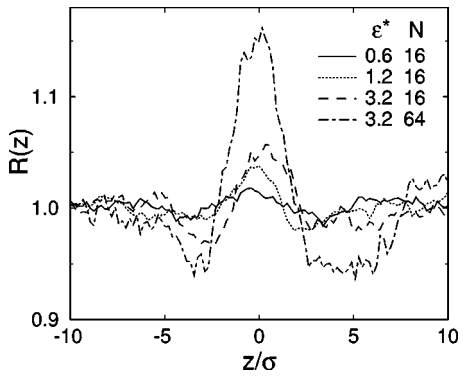

FIG. 2. The relative abundance of chain ends $R(z)$ as a function of height z for the indicated ϵ^* and N. The tendency for chain ends to lie at the interface increases with both ϵ^* and N. Only the region near the interface is shown.

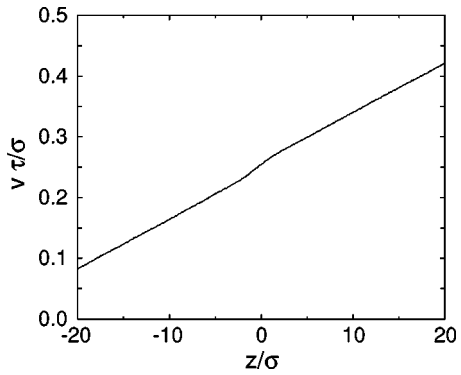

FIG. 3. Average velocity as a function of height z for an upper wall velocity of $0.5\sigma/\tau$. The average was over slices of width 0.25σ parallel to the x-y plane. The polymers had length $N=16$ and $\epsilon^*=3.2$. The slight change in slope in the center implies a lower viscosity near the interface.

terface. This effect can be understood by focusing on an A polymer at the interface. If a middle segment of the A chain is on the B rich side of the interface, then both adjacent A monomers on the chain also have a high probability of interacting with B monomers. However, an end segment of the A chain has only one neighbor that must interact with B monomers. Thus chain ends should have a lower free energy in the interfacial region.

The relative abundance $R(z)$ of chain ends can be measured by taking the ratio of the local concentration of chain ends to the average concentration $2/N$. Figure 2 illustrates how this quantity depends on N and ϵ^*. In all cases, the relative abundance approaches unity far from the interface. There is a peak at the center of the interface that grows as ϵ^* or N increases. To either side of the interface there are small decreases in the abundance of the chain ends. Presumably this is because chain ends are attracted to the center of the interface and the monomers adjacent to them are more likely to be at nearby values of z. The increase in abundance of chain ends near the interface can be expected to reduce the local viscosity, because it reduces the degree to which chains on opposite sides of the interface are intertwined.

B. Flow profiles and boundary conditions

Figure 3 shows the average velocity profile for chains of length $N=16$ at $\epsilon^*=3.2$. Here the x component of the velocity v_x was averaged over all monomers in slices of width 0.25σ parallel to the x-y plane for an interval of 9375τ. A small increase in the slope $\partial v_x/\partial z$ can be seen at the interface $(z=0)$. This implies a decrease in the viscosity of the interface relative to that of the bulk, since the shear stress P_{xz} is independent of z in steady state [21].

Macroscopic treatments of fluid flow typically include the effect of interfaces as boundary conditions on continuum equations. In Fig. 3 the velocity profiles from the bulk A and bulk B regions would extrapolate to different velocities at the interface. This velocity difference is called the slip velocity Δv. In the low velocity limit, Δv is proportional to the bulk shear rate. One can define a shear-rate-independent slip length $S=\Delta v/\dot{\gamma}_B$. This corresponds to the extra width of bulk fluid that would be needed to accommodate the same velocity difference as the interface. Another common measure of slip is the extrapolation length [5,7] which is just half of S.

In most calculations the slip length and velocity are assumed to be zero. This is appropriate as long as the slip length is much smaller than the dimensions of the system being modeled. Table II gives values of S for the systems considered here. Note that S rises with both the immiscibility parameter ϵ^* and N. These trends reflect changes in the relative viscosity of the bulk and interface as discussed below. The largest value obtained is a little above 10σ which corresponds to roughly 5 nm. This is much less than the dimensions of typical pipes and nozzles, but slip lengths of this magnitude are relevant to the operation of nanodevices. In addition, increasing N into the entangled regime would lead to very rapid increases in S [4,5,7].

The presence of a mixture of different species adds an extra complexity to the boundary condition at an interface. In recent work, Koplik and Banavar [25] have considered the

TABLE II. Interfacial slip length S, as a function of ϵ^* and chain length N.

N	ϵ^*	S/σ
64	0.37	4.8 ± 0.5
	0.6	8.5 ± 0.9
	1.2	9.0 ± 0.5
	3.2	12.1 ± 0.5
32	0.37	1.88 ± 0.08
	0.8	2.05 ± 0.13
	1.2	3.45 ± 0.2
	3.2	4.75 ± 0.50
16	0.37	0.68 ± 0.11
	0.8	0.78 ± 0.07
	1.2	1.23 ± 0.2
	3.2	1.67 ± 0.05
8	0.8	0.15 ± 0.05
	1.2	0.30 ± 0.05
	3.2	0.48 ± 0.09

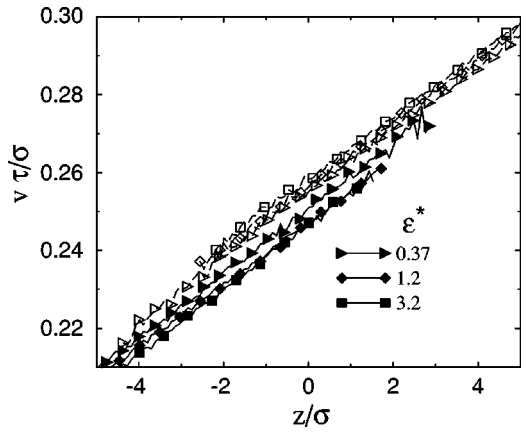

FIG. 4. Average velocity for each species as a function of z for the indicated values of ϵ^*. Open (closed) symbols indicate species A (B) and only the interfacial region is shown. There is a clear difference between the velocities of the two species that increases as ϵ^* increases.

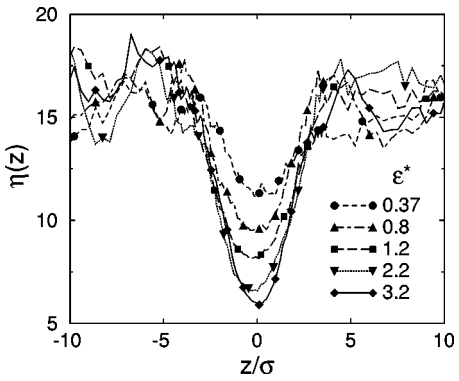

FIG. 5. Viscosity as a function of height z for the $N=32$ polymers as a function of ϵ^*. The viscosity of the bulk regions on either side of the interface is the same, and independent of ϵ^*. The drop in viscosity at the interface is greater as ϵ^* increases.

appropriate flow boundary condition for a fluid mixture near a solid surface. They concluded that the velocities of the different fluid components should be equal to each other near the surface. One might thus expect that the velocities of the two components near a fluid-fluid interface should also be equal. However, we find that this is not the case.

Figure 4 shows flow profiles obtained by taking separate averages over the monomers of each species within a slice. Note that the profiles for the two species remain quite different over the entire range where the concentrations are high enough to measure both velocities with reasonable statistics. Within statistical errors, the slope of each profile is equal to the bulk shear rate. However, the curves are separated by a z-independent shift that grows with the immiscibility parameter ϵ^*. This jump in velocity corresponds to the slip velocity Δv discussed above.

A difference between the velocities of different species at the same height may seem counterintuitive. However, the A and B monomers in the interfacial regions are attached to chains that lie predominantly on opposite sides of the interface. Their average velocity must equal the center of mass velocity of their chain and thus they will tend to move at different velocities. It is well known that shear of bulk polymers leads to a sort of end-over-end rolling of the molecules. Segments that are at low velocities fall behind the center of mass. This creates an increased drag that pulls them back up into regions of higher velocity. Thus at any given height the mean velocity of segments from chains whose centers of mass are at regions of higher velocity is higher than that of those whose center of mass is moving more slowly. A similar rolling must occur at the interfaces in our simulations, although it will be modified due to the change in chain statistics. One may also expect that it will occur in the situation considered by Koplik and Banavar [25], when the fluids consist of chain molecules rather than Lennard-Jones spheres. If one of the species is preferentially attracted to a solid wall, those chains will tend to have centers of mass that lie closer to the wall. One can expect that this will create a difference in the velocity of monomers of the two types in the region near the wall that is analogous to the jump seen in Fig. 4.

C. Interfacial viscosity

Figure 5 shows the variation of $\eta(z)$ [Eq. (6)] with z for $N=32$ and different values of the immiscibility parameter. Far from the interface the local viscosity is equal to the bulk value η_B. This is the same for the two polymers because they have identical masses and interactions. There is a sharp drop in viscosity at the interface that deepens as the fluids become more immiscible. This dip reflects the increase in the slope of the flow profile (e.g., Fig. 3) in the interfacial region. Its integral is directly related to the slip length through

$$S=\int dz\left[\frac{\eta_B}{\eta(z)}-1\right]=\int\frac{dz}{\dot{\gamma}_B}\left[\frac{\partial v_x}{\partial z}-\dot{\gamma}_B\right]=\frac{\Delta v}{\dot{\gamma}_B}. \qquad (8)$$

Increasing ϵ^* increases the magnitude of both the dip in viscosity and the slip length. Thus the trends in Table II parallel those in the figures we now discuss.

One of the key predictions of de Gennes and co-workers [5] and of Goveas and Fredrickson [7] is that the interfacial viscosity should become independent of N when the interface width is small compared to R_g. Figure 6 shows viscosity profiles for different chain lengths at (a) $\epsilon^*=1.2$ and (b) $\epsilon^*=3.2$. The bulk viscosities are proportional to chain length, indicating that the chains can be described by the Rouse model [10]. As predicted [5,7], the interfacial velocity becomes independent of N for sufficiently large N. As ϵ^* increases, the interface width decreases and the interfacial viscosity saturates at smaller values of N. In Fig. 6, the viscosities for $N\geqslant 32$ coincide at $\epsilon^*=1.2$ and values for $N\geqslant 16$ coincide at $\epsilon^*=3.2$.

Figure 7 shows the inverse interfacial viscosity evaluated at the center of the interface for each N as a function of ϵ^*. Results for $N=8$ remain above the other curves for all ϵ^*, but the other curves converge as ϵ^* increases. Using the values from Table I we see that the interface width must be less than about $1.5R_g$ for the interfacial viscosity to saturate.

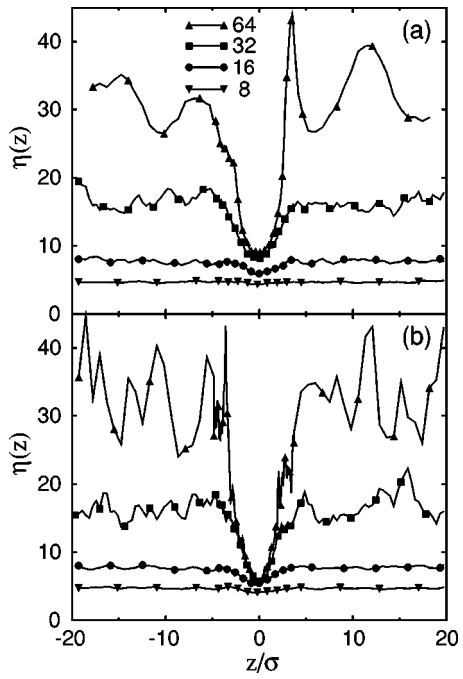

FIG. 6. Viscosity as a function of height z at (a) $\epsilon^*=1.2$ and (b) $\epsilon^*=3.2$. As expected for Rouse polymers, the bulk viscosity of the chains scales linearly with N. In part (a), the viscosity of the $N=32$ and $N=64$ polymers is the same at the interface, indicating that at the interface there is only one length scale common to these two polymer lengths. In part (b) the viscosity for $N=16,32,64$ converges at the interface, which indicates that the interfacial length scale is the same for these three polymer lengths. The statistical fluctuations in the data decrease as the inverse square root of the total strain in a given region. Thus they are smallest in the interfacial region where the shear rate is highest and largest for the longest chains.

This suggests that the radius of gyration of the segments that enter the interface is given by $a_I/1.5$ in the large N limit.

The work of de Gennes and co-workers [5] and of Goveas and Fredrickson [7] predicts that the interfacial viscosity should saturate at a value corresponding to the bulk viscosity of Rouse chains whose radius of gyration is of order the

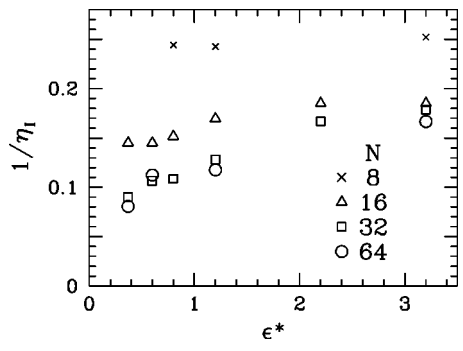

FIG. 7. Inverse interfacial viscosity $1/\eta_I$ as a function of ϵ^* for the indicated N. The $N=64$ and $N=32$ polymers have the same value of η_I for $\epsilon^*\geqslant 0.6$. Values for $N=16$ merge with results for longer chains when $\epsilon^*\geqslant 2.2$. Error bars are comparable to the symbol size.

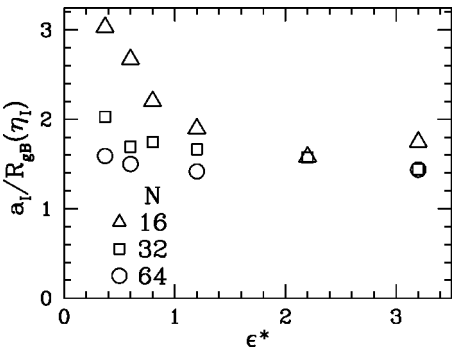

FIG. 8. Variation with ϵ^* in the ratio between the interfacial width and $R_{gB}(\eta_I)$ the radius of gyration of polymers whose bulk viscosity equals η_I. Error bars are comparable to the symbol size.

interface width. To test this we calculated $R_{gB}(\eta_I)=[\nu_0\eta_I/6\zeta]^{1/2}$, the radius of gyration corresponding to a polymer whose bulk viscosity is equal to η_I, using the value of $\zeta=(0.38\pm 0.03)m/\tau$ we determined from bulk regions. Figure 8 shows the ratio $a_I/R_{gB}(\eta_I)$ as a function of ϵ^* for $N=16$, 32, and 64. As expected from the analytic predictions, the ratio approaches a constant value in the limit of large ϵ^*. Moreover, the limiting value of about 1.6 is consistent with the ratio between a_I and R_g at which the inverse viscosity became independent of chain length in Fig. 7. Thus our results confirm that the interfacial viscosity is given by the bulk viscosity of chains whose length is equal to that of the segments that enter the interfacial region. They further imply that these segments have a radius of gyration of about $a_I/1.6$.

IV. SUMMARY AND CONCLUSIONS

In this paper we have presented molecular dynamics simulations of phase separated immiscible polymers. The strength of the immiscibility of the polymers, ϵ^*, was varied from slightly immiscible to well into the immiscible phase. The interfacial width (Table I) decreased with increasing immiscibility. As predicted by Helfand, Bhattacharjee, and Fredrickson [24], the tendency for chain ends to lie at the interface increased with the degree of immiscibility (Fig. 2).

The linear viscous response of the interface to a perpendicular velocity gradient was examined as a function of chain length and immiscibility. Plots of the average velocity as a function of z show an increased slope in the interfacial region (Fig. 3). This implies that a slip boundary condition must be used in continuum theories of sheared polymer blends. The degree of slip was quantified by calculating the slip length S (Table II) which represents the excess width of bulk polymer needed to accommodate the same amount of slip as the interface. Slip has little effect on calculated flow profiles when S is small compared to the system size. For the parameters considered here, the largest values of S are a little greater than 10σ. Thus slip would be irrelevant in macroscopic flows, but might be important in nanodevices. Much larger values of S would be found for entangled polymers.

We found that the average velocities of the two species were different in the interfacial region (Fig. 4). This was

attributed to the fact that the centers of mass of A and B polymers lay on different sides of the interface and moved at different mean velocities. Recent simulations of spherical molecules near solid walls indicated that the two species always had the same velocity [25]. It would be interesting to see if this condition breaks down for longer chain molecules.

The ratio of the bulk to interfacial viscosity and the degree of slip both increased with increasing N and ϵ^*. de Gennes and co-workers [5] and Goveas and Fredrickson [7] had noted that when a_I is sufficiently small compared to R_g the length s^* of the polymer segments that enter the interfacial region is independent of N. They then argued that the interfacial viscosity should scale with the bulk viscosity of polymers of length s^*. Our results are completely consistent with this picture. The value of the interfacial viscosity saturated when the radius of gyration of the chains exceeded about $1.5a_I$ (Fig. 5). Moreover, the saturated value corresponded to the bulk viscosity of chains whose radius of gyration is about $1.6a_I$ (Fig. 8). This suggests that the interfacial viscosity is very nearly equal to that of bulk polymers with length s^*. The only discrepancy with earlier theories is that Goveas and Fredrickson had predicted a substantially smaller prefactor in the relation between s^* and η_I. It would be interesting to explore the origin of this discrepancy in future analytic work.

ACKNOWLEDGMENTS

Discussions with G. Fredrickson, J. Goveas, and M.-D. Lacasse were helpful, and we thank them. We also thank J. Hutter for comments on the manuscript. Support from the Semiconductor Research Corporation, the Department of Energy, and National Science Foundation Grant Nos. DMR-9634131 and DMR-0083286 is gratefully acknowledged. We are also grateful to Intel Corporation for donating workstations that were used in this study.

[1] P. Flory, *Principles of Polymer Chemistry* (Cornell University Press, Ithaca, NY, 1953).
[2] J.W. Cahn and J.E. Hilliard, J. Chem. Phys. **28**, 258 (1958).
[3] E. Helfand and Y. Tagami, J. Chem. Phys. **56**, 3592 (1971).
[4] H. Furukawa, Phys. Rev. A **40**, 6403 (1989).
[5] P.G. de Gennes, C. R. Acad. Sci., Ser. II: Mec., Phys., Chim., Sci. Terre Univers **308**, 1401 (1989); F. Brochard-Wyart, P.G. de Gennes, and S. Troian, *ibid.* **310**, 1169 (1990); P. G. de Gennes in *Physics of Surfaces and Interfaces*, edited by I. C. Sanchez (Butterworth-Heinemann, Boston, 1992).
[6] Y. Rabin and H.C. Öttinger, Europhys. Lett. **13**, 423 (1990).
[7] J.L. Goveas and G.H. Fredrickson, Eur. Phys. J. B **2**, 79 (1998).
[8] O.F. Olaj, T. Petrik, and G. Zifferer, J. Chem. Phys. **108**, 8214 (1998); **108**, 8226 (1998).
[9] M. Müller, Macromol. Theory Simul. **8**, 343 (1999).
[10] M. Doi and S. F. Edwards, *The Theory of Polymer Dynamics* (Clarendon, Oxford, 1986).
[11] K. Kremer and G.S. Grest, J. Chem. Phys. **92**, 5057 (1990).
[12] G.S. Grest, M.-D. Lacasse, K. Kremer, and A.M. Gupta, J. Chem. Phys. **105**, 10 583 (1996).
[13] M.-D. Lacasse, G.S. Grest, and A.J. Levine, Phys. Rev. Lett. **80**, 309 (1998).
[14] M. Allen and D. Tildesley, *Computer Simulations of Liquids* (Oxford University Press, Oxford, 1987).
[15] M. Pütz, K. Kremer, and G.S. Grest, Europhys. Lett. **49**, 735 (2000).
[16] Note that this value of N_e is for a slightly different density ($\rho=0.85\sigma^{-3}$) and temperature ($k_BT/\epsilon=1.0$) than our simulations. However, changes due to these differences are expected to be smaller than the quoted error bars.
[17] P.A. Thompson and M.O. Robbins, Phys. Rev. A **41**, 6830 (1990).
[18] P.A. Thompson and S.M. Troian, Nature (London) **389**, 360 (1997).
[19] R. Khare, J.J. de Pablo, and A. Yethiraj, Macromolecules **29**, 7910 (1996); J. Chem. Phys. **107**, 2589 (1997).
[20] E. Manias, I. Bitsanis, G. Hadziioannou, and G. ten Brinke, Europhys. Lett. **33**, 371 (1996).
[21] Any difference in the values of P_{xz} in different layers implies a net lateral force on the intervening volume. This would lead to an acceleration and imply that the system is not in steady state.
[22] Z. Xu, J.J. de Pablo, and S. Kim, J. Chem. Phys. **102**, 5836 (1995).
[23] M. Sferrazza, C. Xiao, R.A.L. Jones, D.G. Bucknall, J. Webster, and J. Penfold, Phys. Rev. Lett. **78**, 3693 (1997).
[24] E. Helfand, S.M. Bhattacharjee, and G.H. Fredrickson, J. Chem. Phys. **91**, 7200 (1989).
[25] J. Koplik and J.R. Banavar, Phys. Rev. Lett. **80**, 5125 (1998).